energies

MDPI

Article

A Numerical Model of Biomass Combustion Physical and Chemical Processes

Ion V. Ion, Florin Popescu *, Razvan Mahu and Eugen Rusu

Faculty of Engineering, "Dunarea de Jos" University of Galati, 47 Domneasca St., 800008 Galati, Romania; ion.ion@ugal.ro (I.V.I.); razvan.mahu@ugal.ro (R.M.); eugen.rusu@ugal.ro (E.R.)
* Correspondence: florin.popescu@ugal.ro; Tel.: +40-726377053

Abstract: Identifying a modeling procedure of biomass thermal decomposition that is not only simple enough to implement and use, and computationally efficient, but also sufficiently accurate for engineering design activities, and with a spectrum of applications as broad as possible is a very difficult task. The authors propose a procedure which consists of two main stages: (a) the static modeling phase with the purpose of generating the algorithm (macro functions) that supplies a Computational Fluid Dynamics (CFD) model with specific input data (source/sink terms and local material properties) and (b) the dynamic modeling phase, where the CFD model is bi-directionally coupled to the external biomass decomposition model in the form of a User-Defined Function (UDF). The modeling approach was successfully validated against data obtained from single particle decomposition experiments, demonstrating its applicability even to large biomass particles, under high heating rates and combusting conditions.

Keywords: biomass; combustion; decomposition; modeling; numerical simulation

Citation: Ion, I.V.; Popescu, F.; Mahu, R.; Rusu, E. A Numerical Model of Biomass Combustion Physical and Chemical Processes. *Energies* **2021**, *14*, 1978. https://doi.org/10.3390/en14071978

Academic Editor: Rajender Gupta

Received: 2 March 2021
Accepted: 31 March 2021
Published: 2 April 2021

1. Introduction

The work presented herein is entirely founded on the mathematical model of biomass combustion physical and chemical processes explained in great detail in [1]. For a more complete understanding and easier assessment of this effort, we strongly encourage the reader to take it into consideration.

The main goal of this study (the previous and the current paper, together) is to present a possible solution for modeling and simulating biomass thermal decomposition regardless of particle size and shape, heating rate, and neutral or oxidizing environment conditions. Moreover, it is formulated such that any biomass source can be used, provided it can be described using its main constituents (fractions of hemicellulose, cellulose, lignin, minerals, and moisture).

The first paper detailed the complete path starting from the mathematical formulation of the kinetic-chemical model for biomass transformation, and the physical modeling of biomass properties. It concluded by showing the outcome of the decomposition model, in the form of transfer functions to be implemented in the three-dimensional Computational Fluid Dynamics (CFD) model—the static modeling phase.

This second paper presents the subsequent dynamic modeling phase, involving the actual numerical simulation of biomass thermal decomposition and volatiles & char combustion, as well as its verification and validation. The model consists of an external User-Defined Function (UDF) coupled to the CFD numerical model. Introduction of the structure and functionality of the UDF routines, used for calculating the yield rates for decomposition products, the volatiles chemical composition, and the overall process heat balance is followed by the presentation of the modeling and numerical simulations performed to test and validate the numerical model of combustion, whose structure is presented in the first part of this paper. In addition, routines for calculating material properties of raw biomass and solid residue and a calculation model for the radiation absorption coefficient in the

gas phase are included. The basic numerical flow modeling aspects are described, specifically the Reynolds-averaged Navier–Stokes flow model, with the associated turbulence modeling aspects. Chemical reactions and radiation heat transfer modeling, as essential global model components, are then examined. Next, some issues related to the numerical simulation process are discussed, i.e., computational domain modeling and discretization, boundary conditions, numerical solvers, and spatial and temporal discretization schemes.

Numerical tests were run for observing the model behavior strictly for biomass particles drying and devolatilization stages, using various initial moisture levels and external neutral gas flow rates. Both two-dimensional approximations and three-dimensional models have been used, and the results were compared to the available experimental data.

Finally, the paper examines the simulation results of decomposition in an oxidizing atmosphere under the same conditions of thermal load, this time examining the combustion model performance. Cylindrical biomass particles with different shapes were used. All combustion simulation tests have been run using three-dimensional numerical models.

The experimental data published by Lu [2] was chosen for assessing the overall modeling performance and accuracy. Other researchers [3–13] have attempted to model and numerically simulate the decomposition of biomass particles, either in isolation or in the form of particle bed, using various approaches. Generally though, the conclusion was that heat and mass transfer dominated processes—involving large particles with high heating rates—proved significantly more difficult to simulate. Dimensionally-reduced models also have difficulties in coping with more complex situations, particularly due to the importance of three-dimensional effects and asymmetries.

Many research efforts (including Lu's) are limited to mass loss and temperature measurements at particular points. Consequently, no validation of volatiles composition could be performed yet. Nevertheless, an interesting and well-detailed example of the effects of using micronized biomass particles on the quality of the volatiles under pyrolitic conditions is given in [14].

2. Numerical Modeling of Physico-Chemical Processes Involved in Biomass Combustion

2.1. External Model Implementation Function

The CFD software (ANSYS Fluent™) includes a significant part of the physical modeling elements needed in biomass combustion numerical modeling. The software provides, besides the mathematical modeling of fluid flow, a porous solid model environment that is well-suited for modeling and simulating flow inside the biomass particle. Transport equations considered are presented in [15], where it can be noticed that an external model can directly modify the source term of each relevant equation: mass sources of primary and secondary volatiles may be included in the continuity equation, those for chemical species standing for volatiles in the corresponding transport equations and the heat balance can be added to the energy conservation equation. Also, ANSYS Fluent™ software allows computation of thermodynamic and transport properties of any species or phase by means of external routines that can represent functions of calculated variables (pressure, temperature, etc.) of any quantity being accessible for the user. The only constraint is that all these information transfers between an external model and the CFD numerical solver must be made through standard macros, which is common practice.

The main objective during the numerical model development was to make extensive use of the existing ANSYS Fluent™ software capabilities and to only integrate the missing parts. Thus, the interaction between basic numerical solver and external transfer function (UDF) has been minimized, which, in a first phase, resulted in a reduced computational time and effort. Moreover, the transfer function code has been optimized, reducing the number of arithmetic operations and embedded routines to a minimum, thus improving the numerical model performance in the second phase. Numerical tests conducted during the research have shown that the extra computational effort for external function processing has not exceeded 10% of the total effort.

The C programming language has been used for UDF programming, with the source file then being compiled into an external dynamic library attached to the numerical solver. UDF compilation ensures faster execution speed and portability.

Table 1 provides an overview on the main operations performed by the transfer function.

Table 1. Main calculations performed by the user-defined function (UDF).

Calculation Type	Purpose
Initialization calculations	Calculate initial concentrations of biomass components Initialize dynamic memory locations for storing current values
Current calculations (performed for each sub-iteration)	Estimate biomass components decomposition rates based on solver-generated local conditions Estimate values for mass sources (chemical species) and energy and transfer to solver Calculate material properties: porosity, viscous resistance coefficients, thermal conductivity, specific heat, and transfer to solver
Closing/final calculations (performed at the end of each time phase)	Recalculate biomass components concentrations using source values at the end of each sub-iteration Calculate biomass current mass and transfer results to a text file

Given that, besides the initialization calculations, all other calculations in Table 1 are performed for each grid cell in the computational domain (the number of operations is therefore directly proportional to the size of the discretization grid) at every time step (current calculations even at each iteration). Thus, it is clearly important to keep the total number of floating point operations under control.

2.2. Fluid Flow, Turbulence, Chemical Reactions, and Radiation Modeling

This chapter provides an overview on mathematical models used for modeling fluid flow and mass and energy transfer, specific to biomass combustion; the other topics will be discussed in Section 2.3.

The Reynolds-averaged Navier–Stokes (RANS) model used for flow modeling is described in [15]. Menter's shear-stress transport *SST* model *k-ω* ("Shear-Stress Transport") has been used for turbulence modeling in all numerical simulations presented in this research paper, as it is considered the most reliable model with two transport equations applicable for both internal and external flows.

Chemical reactions modeling is carried out with the EDC model ("Eddy-Dissipation Concept") [15], which allows introduction of the detailed reaction mechanism in turbulent flows, with the numerical integration of the reactions being carried out by the ISAT algorithm.

A particularly important aspect of general combustion modeling and simulation, not just for biomass, is modeling heat transfer by radiation. The model used for calculating heat fluxes by radiation was the DO model ("Discrete Ordinates"). Its advantage is that it can model optical media of any opacity, which makes it particularly useful for small-sized combustion chambers. The main disadvantage lies in the number of transport equations, which are directly proportional to the number of spatial directions, which limits the applicable angular discretization, especially in three-dimensional modeling. In all 3D cases, a 2×2 discretization has been used for each spherical octant.

The following values have been used in all calculations: 0.8 for raw biomass emissivity and 0.9 for char emissivity. The refractive index of the fluid medium has always been considered equal to one.

Modeling Radiative Heat Transfer Coefficient in the Fluid

Given the importance of heat transfer by radiation, we have considered necessary to model the fluid medium effect on radiation transfer. Therefore, we have included in the combustion numerical model our own model for calculating the gas phase radiation absorption coefficient. The model was developed in Standard C and it is based on data published in [16], section "Heat Transfer by Radiation". The handbook provides equations/correlations for calculating water vapor and carbon dioxide emissivity for several temperatures, as expressions of the following form (the example is given for carbon dioxide):

$$\varepsilon_{CO_2,i}(p,L) = \frac{1}{T_i} 10^{[a_0 + a_1 log(pL) + a_2 log(pL)^2 + a_3 log(pL)^3]} \quad (1)$$

where p is partial pressure of the species [atm], and L the characteristic length [m].

As these equations are given only for three temperatures, namely 1000, 1500, and 2000 K, to avoid interpolation and extrapolation in case of intermediate or higher temperature, we have determined a series of equations where the temperature is a parameter, so it can be directly integrated in the CFD numerical model. Using a second order polynomial regression of the a coefficients in Equation (1), they have been transformed into functions of temperature, as follows:

$$\varepsilon_{CO_2,i}(p,L,T) = \frac{1}{T} 10^{[a_0(T) + a_1(T) log(pL) + a_2(T) log(pL)^2 + a_3(T) log(pL)^3]}. \quad (2)$$

The partial pressure of species can be calculated directly from information available in numerical solver, the characteristic length can be set to a value representative of the simulated facility, and the equivalent emissivity is calculated as the sum of species emissivity. The only parameter to be estimated is the absorption coefficient, calculated in each control volume by Equation (3):

$$a = \frac{-\left[ln\left(1 - \varepsilon_{equiv}\right)\right]}{L}. \quad (3)$$

2.3. Numerical Simulation

2.3.1. Computational Domain. Spatial Discretization Grid

The external boundaries of computational domain (Figure 1) have been modeled considering the characteristics of the experimental chamber furnace described in Section 3.1. Biomass particles were placed in the center, with the same orientation as in the experiments—the cylindrical particle axis parallel to the horizontal direction (the *Z*-axis in the 3D CFD numerical model). In cases of two-dimensional modeling and simulation, the computation domain has been reduced to a section in the XY plane of the original domain.

The numerical simulations have not revealed any dependency between experimental results and finite volumes shape, so the grid contains both 2D triangular and rectangular elements. The main effort was focused on minimizing elements deformation ("skewness") and local growth ratios to reduce the effects of numerical diffusion and improve the accuracy of discretization schemes and gradients calculation. Figure 1b shows smoothness and spatial distribution of mesh nodes used in 2D CFD modeling and simulation.

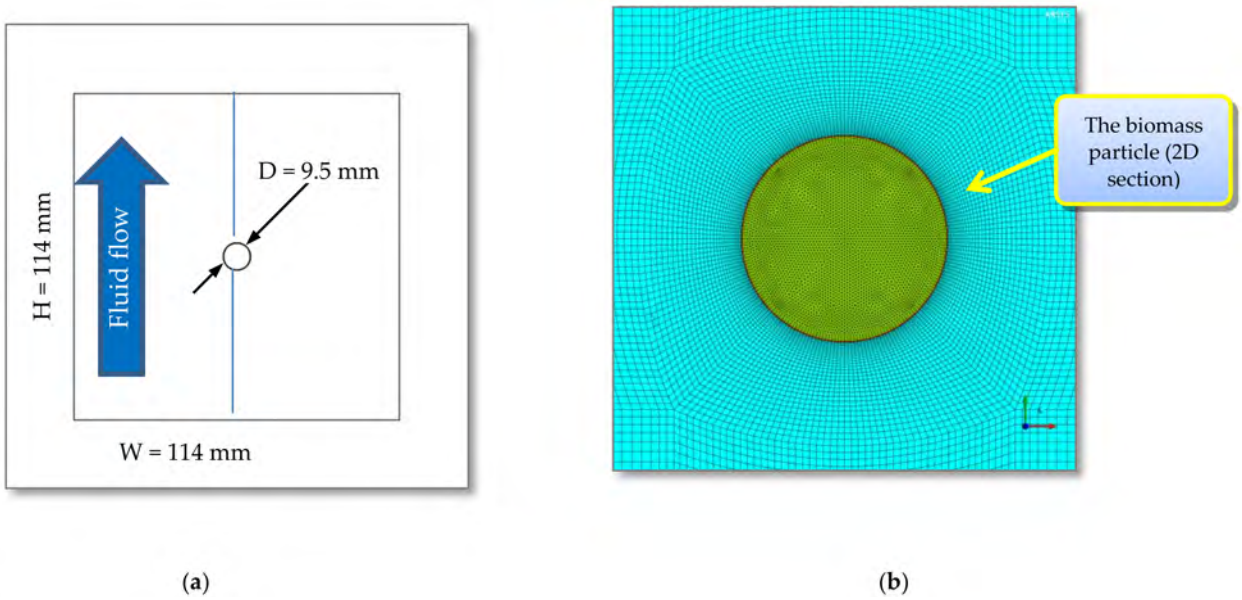

Figure 1. (**a**) Computational domain form and dimensions and (**b**) discretization used in 2D simulations.

Three-dimensional discretization has been used for both cylindrical samples with $L/D = 1$ and for $L/D = 4$.

The multi-block structured discretization technique has been used for all 3D modeling cases. Moreover, taking advantage of the two geometrical symmetry planes of the particle, the 3D computational domain has been reduced to a quarter of its original size, as shown in Figures 2 and 3. The final dimensions of 3D discretization schemes include approximately 135,000 finite volumes for the first particle ($L/D = 1$) and approximately 175,000 finite volumes for the second ($L/D = 4$).

2.3.2. Boundary Conditions

Boundary conditions used in the 2D and 3D numerical simulations are VELOCITY-INLET, PRESSURE-OUTLET, WALL, and SYMMETRY type.

2.3.3. CFD Numerical Solver. Spatial and Temporal Discretization Numerical Schemes

The numerical solver used in all experimental cases is an implicit pressure-based coupled solver. The coupled algorithm is very robust and converges quickly; the only disadvantage lies in the memory size required for storing the coupled equations system.

2.3.4. Discretization of Transport Equations

Among the available schemes, spatial discretization schemes of upwind type of at least second-order accuracy have been used for all simulation cases.

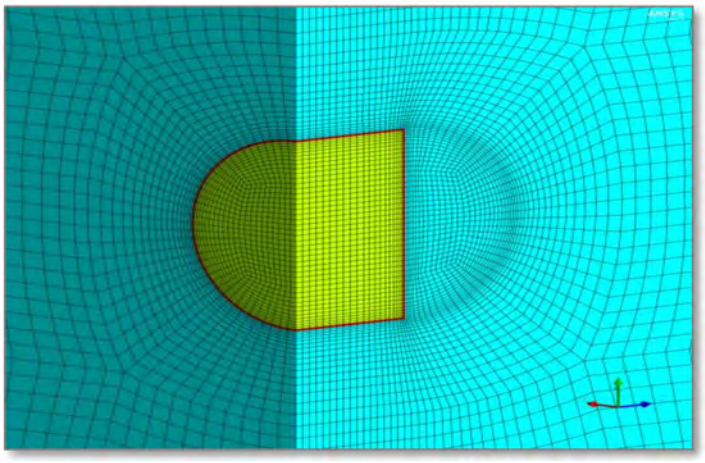

Figure 2. Discretization used in 3D simulations of the particle with *L/D* = 1.

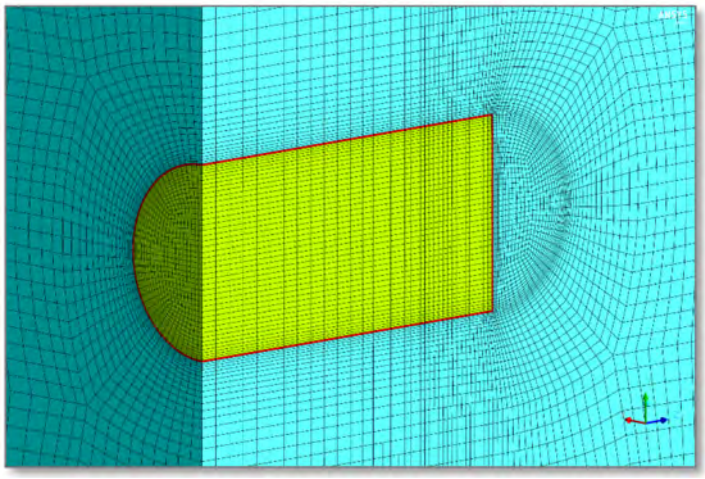

Figure 3. Discretization used in 3D simulations of the particle with *L/D* = 4.

3. Verification and Validation of Biomass Combustion Numerical Model

3.1. Presentation of Validation Experiment

In order to test and subsequently validate the combustion numerical model described in the previous chapters, we searched for experimental data that meet certain criteria: (1) biomass particles considered large enough so that their thermal decomposition regime would be heat and mass transfer dominated; and (2) biomass to be decomposed under high temperature and heating rates. The main argument used to support the selection criteria is that these types of conditions are much more difficult to reproduce numerically; therefore, they are more relevant for testing its behavior. The set of experimental data available in Lu's doctoral thesis [2] meets the requirements and has been used by other authors in their own numerical studies. His experimental furnace has a cylindrical test chamber made of refractory material (SiC). Its total height is 305 mm, with an exterior diameter of 152 mm, and an interior diameter of 114 mm. A vertical hot gas flow passes through the test chamber during the experiments, containing either nitrogen (for pyrolysis experiments), or a mixture of nitrogen and oxygen (for combustion experiments). Experimental measurements have been carried out on cylindrical-shaped biomass samples of various sizes and *L/D* ratios.

3.2. Verification and Validation of Drying and Devolatilization Model

The analysis of the numerical model performance developed in this research paper has been primarily based on particle mass time variation during drying and devolatilization processes. No output gases composition data was available from Lu's experiments. The

model assumes decomposition of two biomass particles with $L/D = 1$ and $L/D = 4$, for which Lu has published experimental results.

The material used for sample manufacturing is poplar wood. We analyzed the cases for a particle moisture content of 6% and 40%.

Although the model has been designed and created to be used primarily for three-dimensional modeling and simulation, tests required during the model development phases have been performed on two-dimensional problems without altering the model structure (in this case, the UDF). The main reason for conducting the tests on 2D CFD models would be the significantly shorter computational time, which allows the running of a greater number of tests within a given timeframe, thus speeding up the development process.

The results obtained with the 2D CFD numerical models were only considered relevant by comparing them with experimental results obtained for the second (higher aspect ratio) particle. However, for validation purposes, these results were neglected and only three-dimensional simulation results were considered.

Taking into consideration the influence of the particles' shape, and geometry of the experimental furnace chamber, and for greater length particles, the ratio between particle length and chamber inner diameter, there is no doubt that 3D modeling was the only way to validate the accuracy of biomass decomposition numerical model.

Three-dimensional effects become readily apparent during experimental data analysis. The most important aspect, namely the particle shape, has a great influence on the decomposition rate. The conversion of the cylindrical-shaped particle with the length equal to its diameter occurs in app. 30 s, as compared to 50 s in the case of the particle with the $L/D = 4$ (Figure 4), for equal diameters (9.5 mm) and the same thermal conditions, with an initial moisture content of 6%.

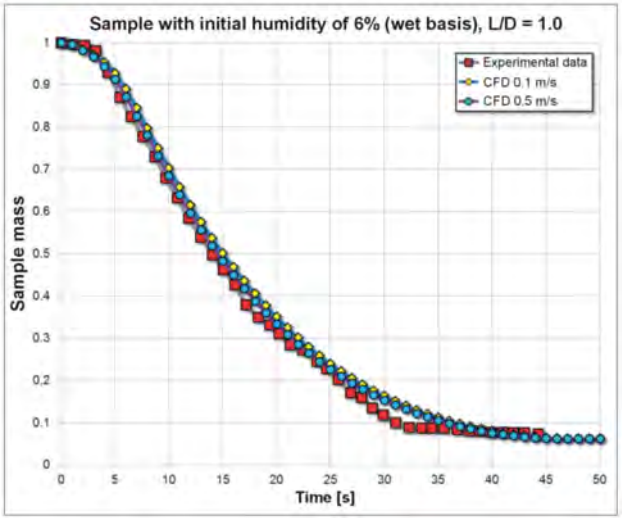

Figure 4. Comparison between simulated and experimental results [2] for pyrolysis of 6% initial moisture sample (determined on wet basis) and $L/D = 1$—3D model.

Modeling and simulation of the shorter particle ($L/D = 1$) was performed for an initial moisture content of 6% (Figure 4) and 40% (Figure 5).

Three-dimensional model accuracy for devolatilization simulation was very good, which was more obvious in the case of low moisture. The slight degradation of the numerical results accuracy in the second phase is most likely due to neglecting contraction. However, the effectiveness in solving this momentary deficiency of the biomass decomposition numerical model should also be noted by applying a correction factor to the empirical correlations used for modeling the thermal conductivity of solid fractions. Again, even the final char fraction was estimated well in both situations.

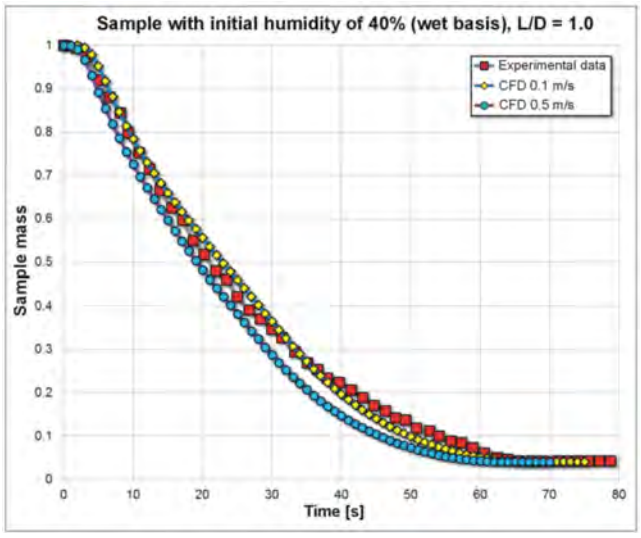

Figure 5. Comparison between simulated and experimental results [2] for pyrolysis of sample with 40% initial moisture (determined on wet basis) and *L/D* = 1—3D model.

As for the longer particle (*L/D* = 4), only the 40% moisture fraction (determined on wet basis) simulation results are discussed. Figure 6 displays both 2D and 3D numerical results. It is obvious that three-dimensional model dimensional accuracy is superior, particularly within the (20–50) s range. This finding confirms the existence of the previously mentioned three-dimensional effects, which are successfully reproduced by the 3D model. This last result obtained under pyrolysis conditions (nitrogen-free atmosphere) concludes the numerical model validation, at least for biomass drying and devolatilization processes and also for char gasification, as the gasification reactions were used in all cases.

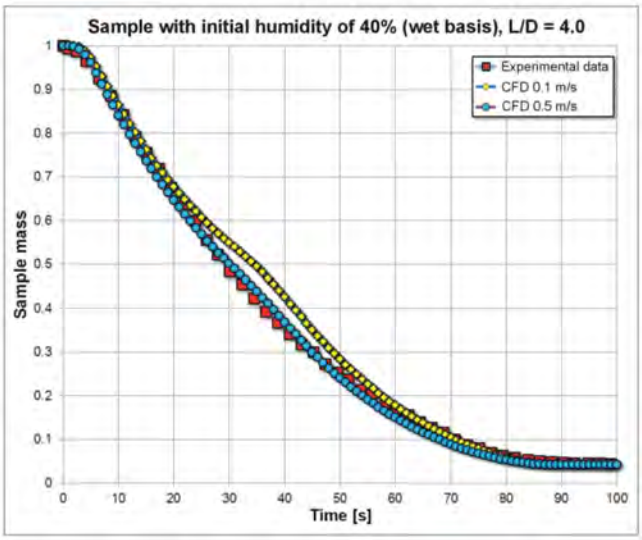

Figure 6. Comparison between simulated and experimental results [2] for pyrolysis of sample with 40% initial moisture (determined on wet basis) and *L/D* = 4—2D/3D model.

An extremely important aspect in assessing model quality is that it was entirely completed in the development phase, where only two-dimensional CFD models were used. In three-dimensional modeling and simulation phase, the numerical model had only been validated and no changes had been made in an attempt to correct or calibrate the results.

3.3. Combustion Model Verification and Validation

From the research data published by Lu [2] only two combustion cases could be identified. Experimental measurements have been carried out in an oxidizing atmosphere for a cylindrical sample with a diameter equal to length (9.5 mm), with 6% and 40% initial moisture (based on the wet mass), respectively but the data on particle mass evolution in time were available only for the high moisture content particle. Flame temperature measurements were nevertheless performed for both particles. At 6% moisture, the temperature was measured both with the external thermocouple and pyrometer camera, the maximum value reached during volatiles combustion was about 2100 K. In the second case, high water content limited the maximum combustion temperature during devolatilization to about 1650 K. Numerical results were obtained only for this second case.

Measured data indicate that complete decomposition occurs in approximately 80 s, with devolatilization stage being complete at about 60 s. The residual mass of experimental particle at the end of conversion is virtually zero, which would indicate complete char combustion. Outside temperature during char combustion was around 1300 K for the first experiment, but reached a value equal to that observed during volatiles combustion for the second experiment. The temperature recorded by the thermocouple in the center of the particle has a maximum value equal to the maximum exterior temperature at the end of conversion (80 s) in both experiments.

The particle decomposition rate (time evolution of relative mass) was again very well reproduced by the numerical model, as shown in Figure 7. Particle residual mass was nevertheless higher than the experimental one. The explanation could be that either: (1) the initial ash fraction from raw biomass, as modeled, was greater than the actual fraction, or (2) the experimental particle ash was effectively swept away by the external gas flow.

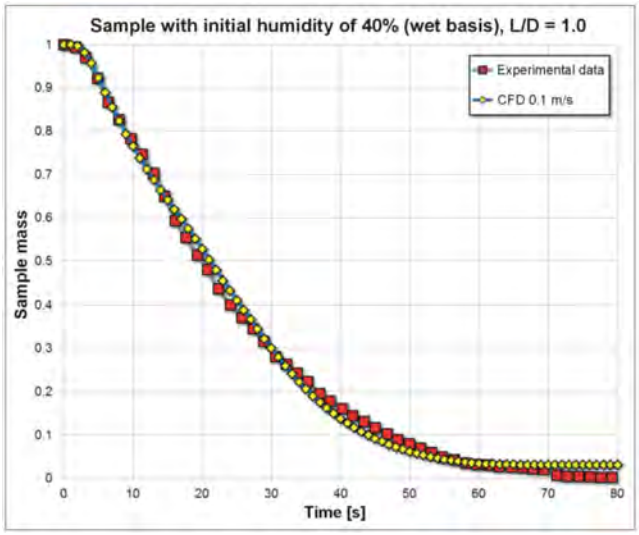

Figure 7. Comparison between simulated and experimental results [2] for the combustion of the sample with 40% initial moisture (wet basis) and *L/D* ratio = 1—3D model.

3.3.1. Combustion of Particle with *L/D* = 1

Some results for the combustion numerical simulation of the *L/D* = 1 sample with 40% initial moisture are presented next. The images show the time history for certain calculated quantities by displaying distributions at different stages in the decomposition process. All images were taken in one of the vertical symmetry planes and mirrored by the orthogonal symmetry plane.

Moisture Drying—Evaporation

Figure 8 shows the gradual evaporation of the initial moisture progressing from the outside to the inside, as the particle is heated. This stage ends at approximately t = 25 s.

Even these early images show the three-dimensional nature of the process, with evaporation in the area of particle sharp edges being much more intense than elsewhere. This feature is characteristic to all other quantities. Water evaporation occurs inwards as an advancing front, whose thickness tends to increase with time. Towards the end, the vaporization occurs across the entire particle core. It is worth mentioning that the model takes into account the transport of water vapors both outwards and inwards, which certainly plays a role in the process.

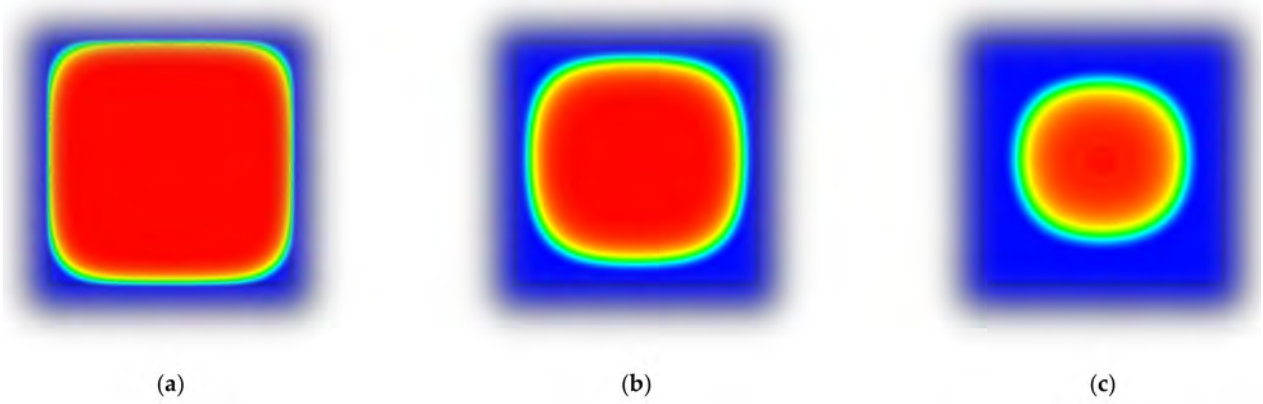

Figure 8. Concentration of initial moisture at (**a**) t = 5 s, (**b**) 10 s and (**c**) 15 s.

Particle Devolatilization

Due to the high thermal gradient, converting biomass components form virgin to active forms, followed by decomposition of the latter, occurs very rapidly in the outer layers of the particle. Process speed is reduced as it moves towards the center of the particle, as shown in Figure 9, mainly due to the thermal resistance of the char layer, which reduces heat flow.

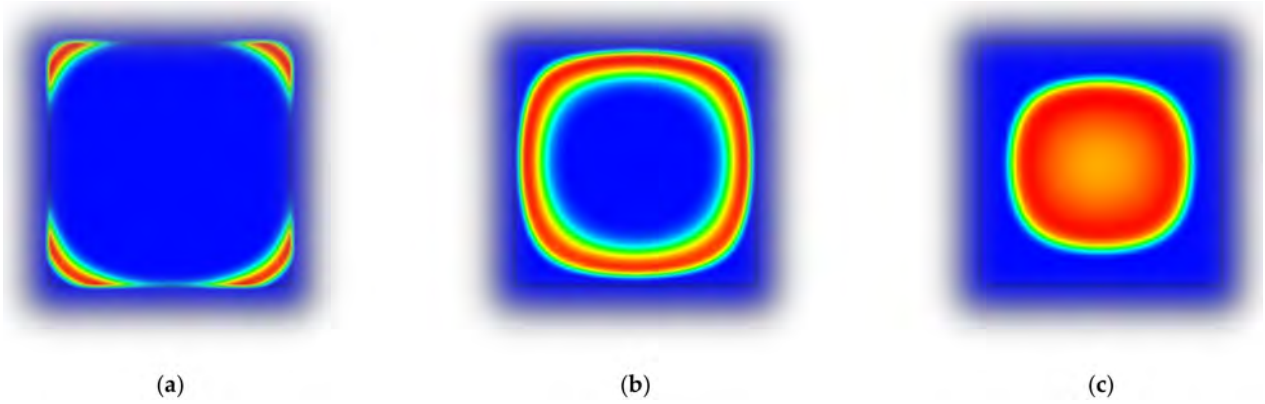

Figure 9. Concentration of "active" cellulose at (**a**) t = 15 s, (**b**) 25 s and (**c**) 35 s.

Char formation (Figure 10) by biomass components decomposition occurs sequentially, with cellulose, hemicellulose and lignin decomposition temperatures and speeds being different. For instance, lignin is the last to decompose at significantly higher temperatures than hemicellulose, which means that the formation of carbon residue can occur simultaneously on a significant fraction of the total particle thickness. However, at the same time, char decomposition occurs due to the combined action of the gasification reactions and, more importantly, the oxidation reaction.

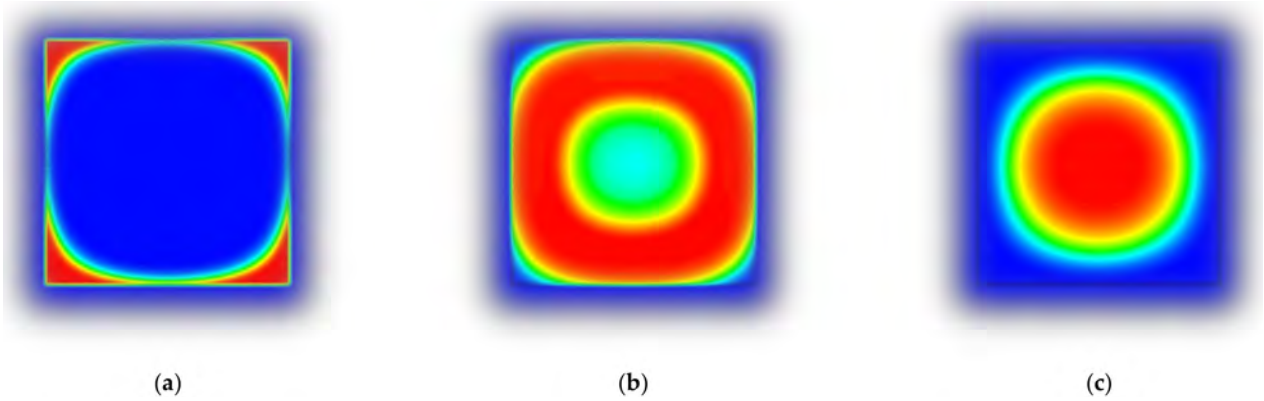

Figure 10. Concentration of char at (**a**) t = 20 s, (**b**) 40 s and (**c**) 60 s.

Figure 10b shows that at 40 s after the start of the numerical experiment, char decomposition started on the edges, while within the particle core, there are fractions of the original biomass components still intact. After 60 s, much of char had already burned, with the process being limited by the oxygen diffusion speed through the remaining ash layer.

Volatiles and Char Burning

Figure 11 shows the instantaneous concentration of the most important species in burnt gas composition immediately after moisture evaporation stage (t = 25 s). The flame temperature in the numerical model is about 1700 K. Maximum species concentrations are: CO = 14%, CO_2 = 19.3%, and H_2O = 1.9%. Water results only from biomass decomposition and burning of molecular hydrogen (in the composition of chemical species, no differentiation is made between fractions of water from different sources) and is quite scarce compared to carbon oxides. CO concentration decreases rapidly after leaving the particle by oxidation to CO_2, but becomes visibly slower about 20 mm above.

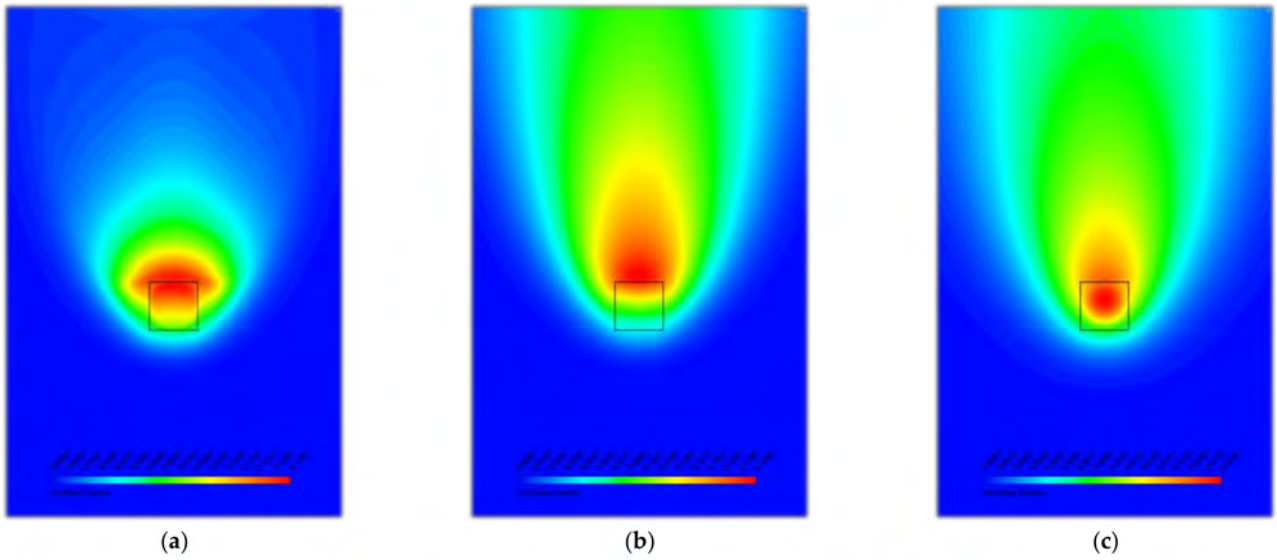

Figure 11. Mass fraction of (**a**)CO, (**b**)CO_2, and H_2O (**c**) at t = 25 s; maximum values: (**a**) 0.1399, (**b**) 0.1926 and (**c**) 0.0192.

Figure 12 shows the same gas species in the final phase (t = 50 s), when most of the biomass has already been converted and the transition is made to the char combustion phase. The maximum concentrations of the species are: CO = 4.84%, CO_2 = 5.45%, and H_2O = 0.3%, three to four times lower compared to the previous time.

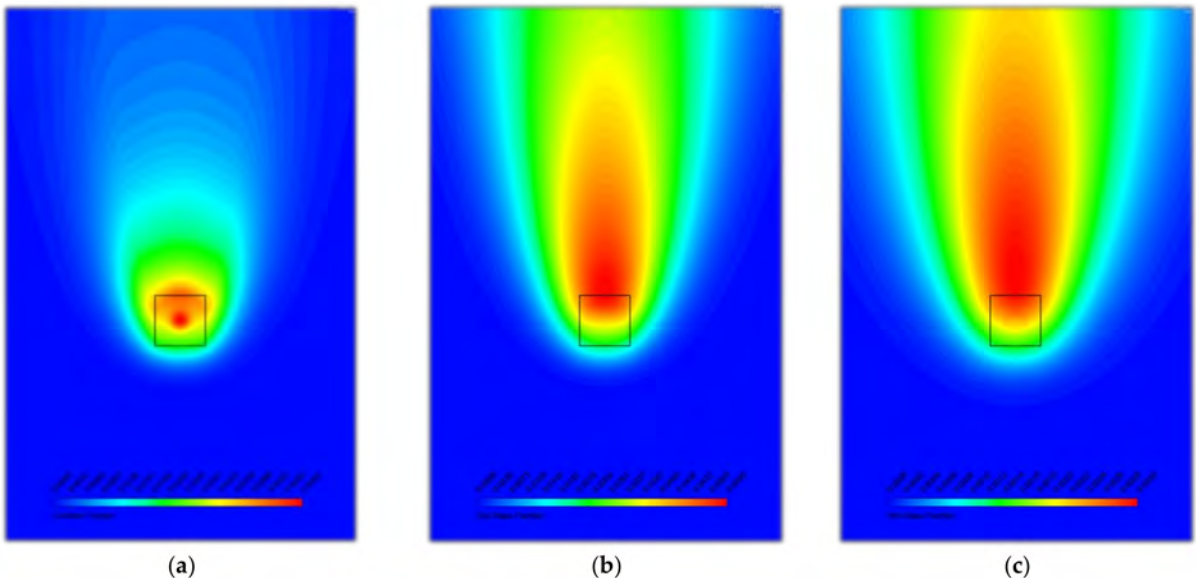

Figure 12. Mass fraction of (**a**) CO, (b) CO_2 and (**c**) H_2O, at t = 50 s; maximum values: (**a**) 0.0484, (**b**) 0.0545 and (**c**) 0.003.

Carbon oxides are dominant again, as expected, water resulting from methane, ethylene, and hydrogen burning and coal decomposition (which contains a certain fraction of H and O, as seen in [1]). CO distribution is much narrower and its conversion into CO_2 occurs on a longer range, with a lower flame temperature (1300 K). It is also obvious that the shape of the area covered by the flow of chemical species leaving biomass particle is slightly modified. This is due to the decomposition rate decrease, which is confirmed by concentration values.

Although the gas stream outside temperature is T = 1050 K, igniting fuel gas mixture from the decomposition of biomass sample only occurs after approximately 15 s. Autoignition was most likely delayed by the cooling effect of the large amount of water that evaporates in the initial stage. The maximum temperature of the flame (≈1700 K) was reached towards the end of the drying step. After t = 25 s the flame continually lost intensity, reaching a minimum at 55 s (T = 1300 K), after which, with accelerating decomposition of the carbon residue reached ≈1500 K at the end of the process. Figure 13 shows how the flame finally covers the entire particle, char combustion making the transition from decomposition regime II to regime I [1].

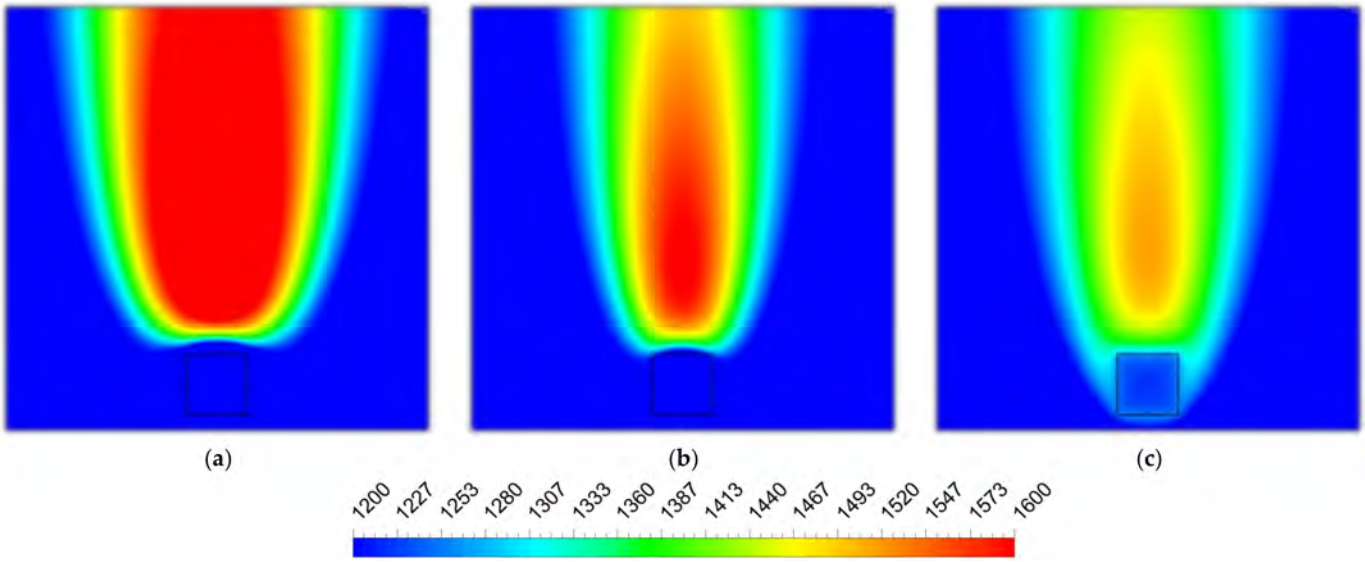

Figure 13. Distribution of temperature (in K) at (**a**) t = 25 s, (**b**) 40 s and (**c**) 75 s.

3.3.2. Combustion of Particle with $L/D = 4$

Although there are no experimental data published by Lu for this case, we have performed combustion modeling and simulation for a particle with the L/D ratio = 4, all other parameters being identical to the previous case. The only possible basis for comparison was the curve of particle mass loss determined in neutral atmosphere. Thus, Figure 14 shows the results of the two 3D numerical simulations, pyrolysis and combustion, superposed on pyrolysis experimental data. The two particle mass loss curves can be seen to begin to evolve differently from $t \approx 23$ s; from this point onwards, the devolatilization is significantly more intense in the case of combustion. This is due to the additional thermal load generated by volatiles burning. Decomposition ends about 20 s earlier and the residual mass of the particle is about 40% lower compared to the pyrolysis case.

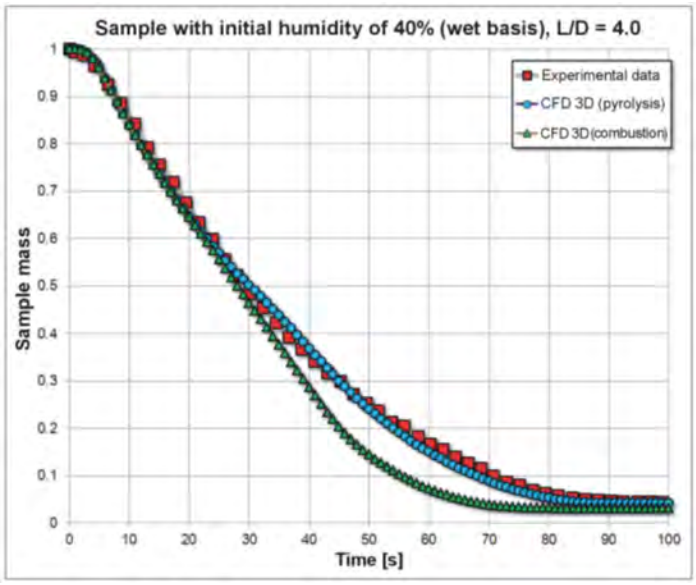

Figure 14. Comparison between simulated and experimental results [2] for the combustion of the sample with 40% initial moisture (compared with wet mass) and $L/D = 4$—3D model.

Moisture Evaporation

Moisture content is the same as in the case of the previous particle ($L/D = 1$) or 40%. Figure 15 shows water evaporation in time, at the same time points. Thickening of evaporation front and a change in shape as it goes deeper is obvious again. In this case, however, the process vertical asymmetry is much more obvious, the process advancing rate being higher on the biomass particle underside. This is obviously caused by the more intense convective heat transfer on the side directly exposed to preheated air flow. This is an effect which can be reproduced only by modeling the external flow also, to allow the calculation of a realistic heat flow distribution on the outside surface of the particle.

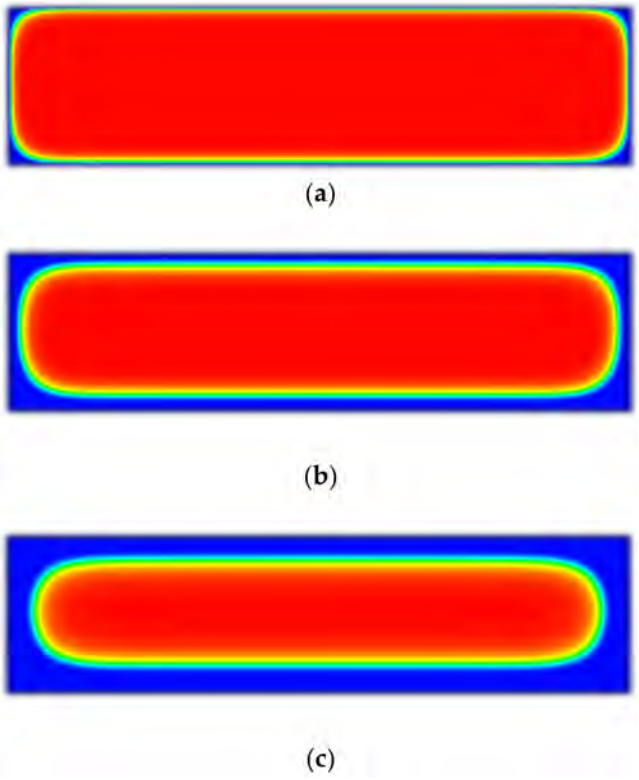

Figure 15. Concentration of initial moisture at (**a**) t = 5 s, (**b**) 10 s and (**c**) 15 s.

Particle Devolatilization

The same thermal decomposition characteristics of biomass components observed for the first particle can be seen in Figure 16: faster transformation at the beginning, followed by a decreased rate during the formation of char, whose thermal conductivity coefficient is, for experimental conditions, 2.5 times lower compared with raw biomass.

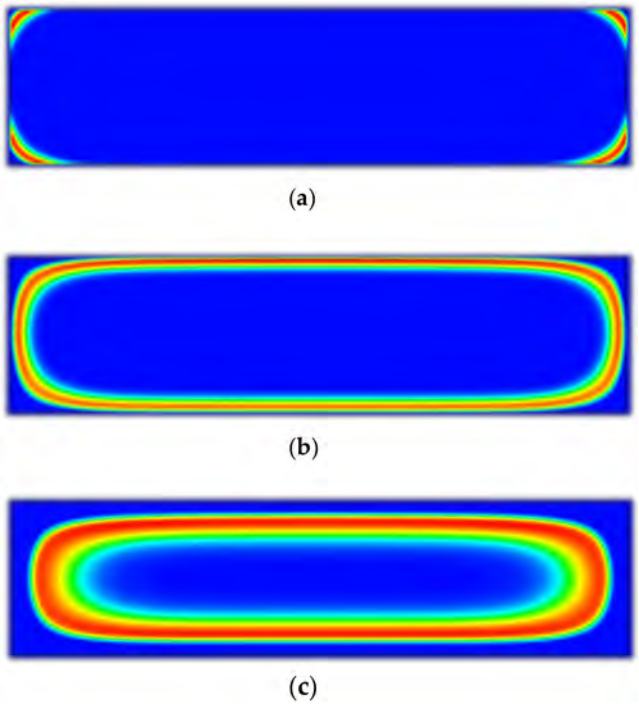

Figure 16. Concentration of "active" cellulose at (**a**) t = 15 s, (**b**) 25 s and (**c**) 35 s.

Compared with the L/D = 1 case, it is noted that at t = 60 s the remaining coal fraction is higher, particularly in the areas close to the lateral surface (for the particle with L/D ratio = 1, coal decomposition occurs in a relatively symmetrical manner, see Figure 10). Char burning appears to be much more intense at particle ends, which is confirmed by residue distribution at t = 75 s, shown in Figure 17d. It seems that oxygen diffusion in the particle solid waste volume occurs much easier towards the ends. This effect might be amplified if the numerical model would also reproduce particle disintegration, reduction of ash layer thickness that would be obvious at the ends, around the sharp edges, etc.

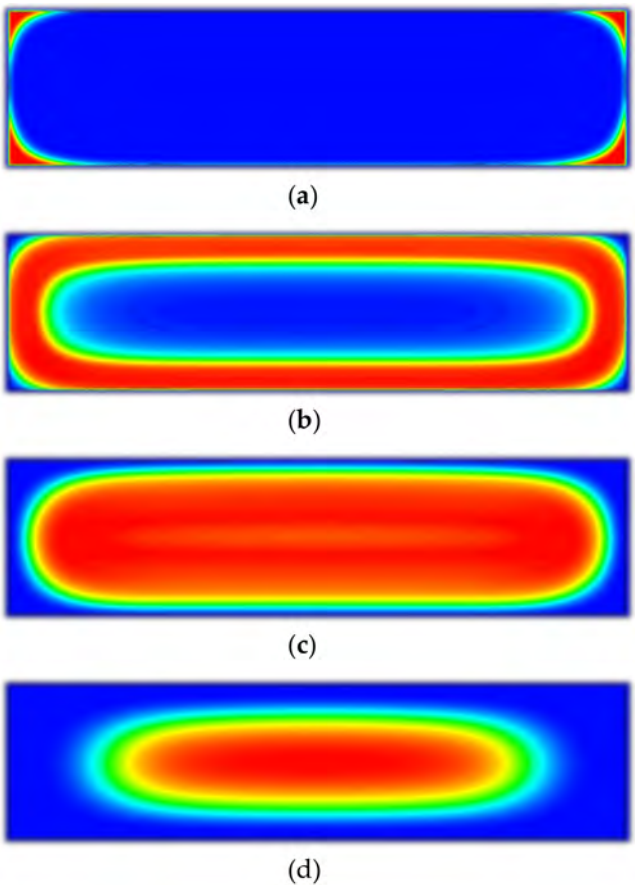

Figure 17. Char residue concentration at (**a**) t = 20 s, (**b**) 40 s, (**c**) 60 s and (**d**) 75 s.

Volatiles and Char Combustion

Figure 18 shows the instantaneous concentrations of the most important chemical species at t = 25 s. Flame temperature in numerical model at this moment is similar to the previous case (≈1700 K). Maximum concentration values are: CO = 14%, CO_2 = 23.2%, and H_2O = 20.1%. The large water fraction yields are caused by the incomplete initial moisture drying at this point (the maximum value occurs actually in the particle core). Rapid carbon monoxide oxidation is also obvious here.

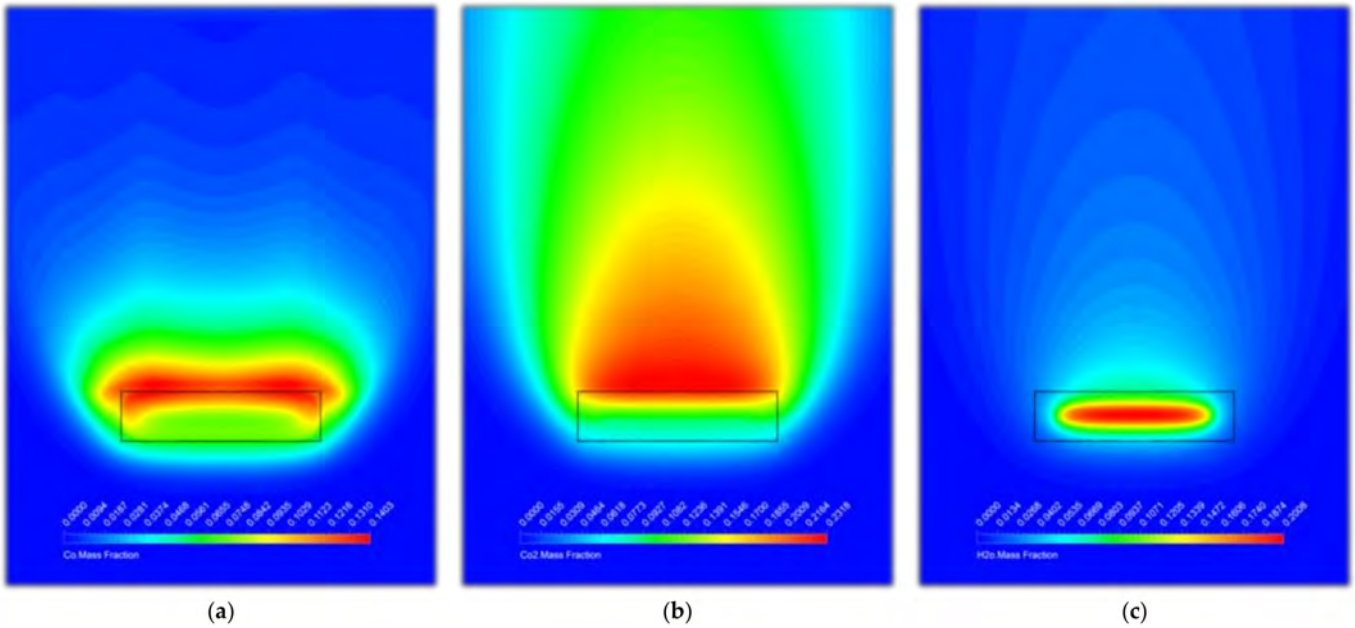

Figure 18. Mass fraction (**a**) CO, (**b**) CO_2 and (**c**) H_2O at t = 25 s; maximum values: (**a**) 0.1403, (**b**) 0.2318 and (**c**) 0.2008.

Figure 19 shows the same species at t = 50 s, when, unlike the first particle, there is still an important fraction of unconverted biomass. Maximum values of species concentrations are: CO = 13.6%, CO_2 = 24.2%, și H_2O = 2.1%, similar values to the previous time moment, with the exception of water. Flame temperature at this stage is ≈1800 K.

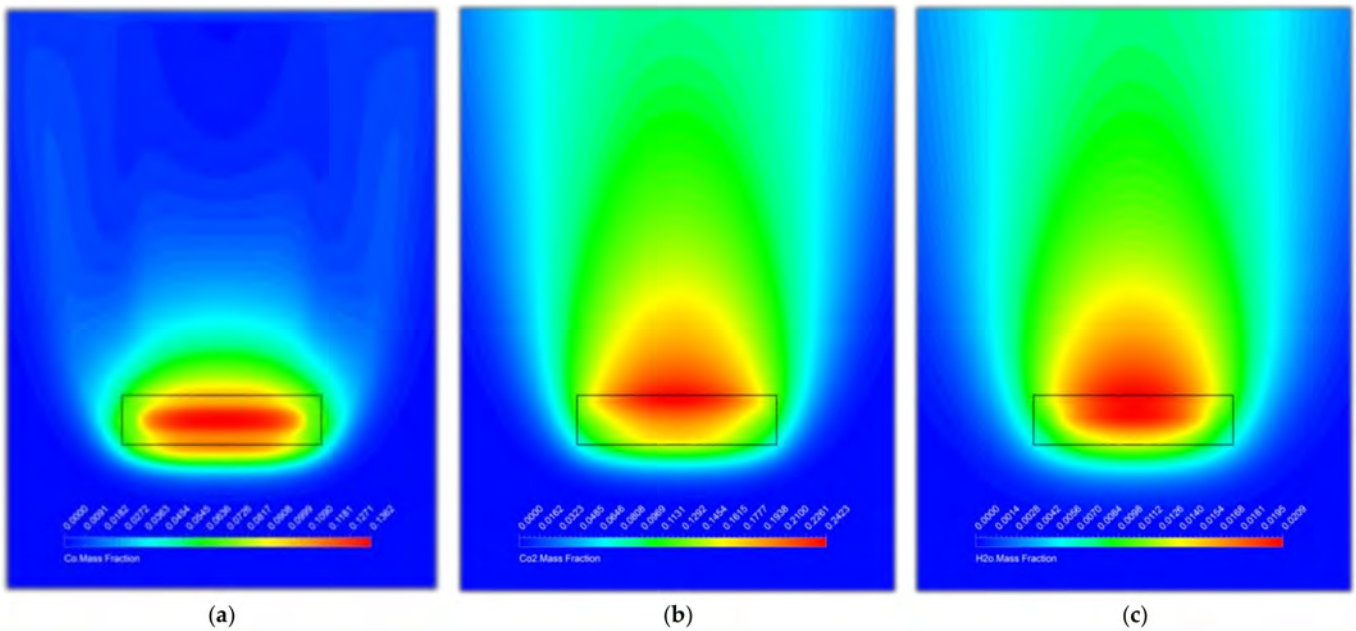

Figure 19. Mass fraction (**a**) CO, (**b**) CO_2 and (**c**) H_2O at t = 50 s; maximum values (**a**) 0.1362, (**b**) 0.2423 and (**c**) 0.0209.

Again, fuel gas mixture resulting from the biomass sample decomposition ignites late, only after approximately 18 s. The maximum flame temperature (≈2200 K) occurs this time during char combustion. During volatiles burning the maximum temperature reaches 1800 K. Burning intensity reduction is obvious for the second particle as well, with the minimum being at t = 65 s when the temperature reaches approximately 1550 K. Figure 20 shows that not only is the temperature evolution different during combustion, but also the flame shape, which was however predictable. Combustion is more intense towards particle ends, with the flame being shaped like a double cone. At t = 40 s, it should be noted the

flame length has reduced and temperature increased as compared with 15 s earlier, one of the reasons being the completion of the drying phase. During char burning, the flame returns to the simple conical shape, with oxidation being much more intense as compared with the first particle (judging not only by the flame shape, but also by the temperature).

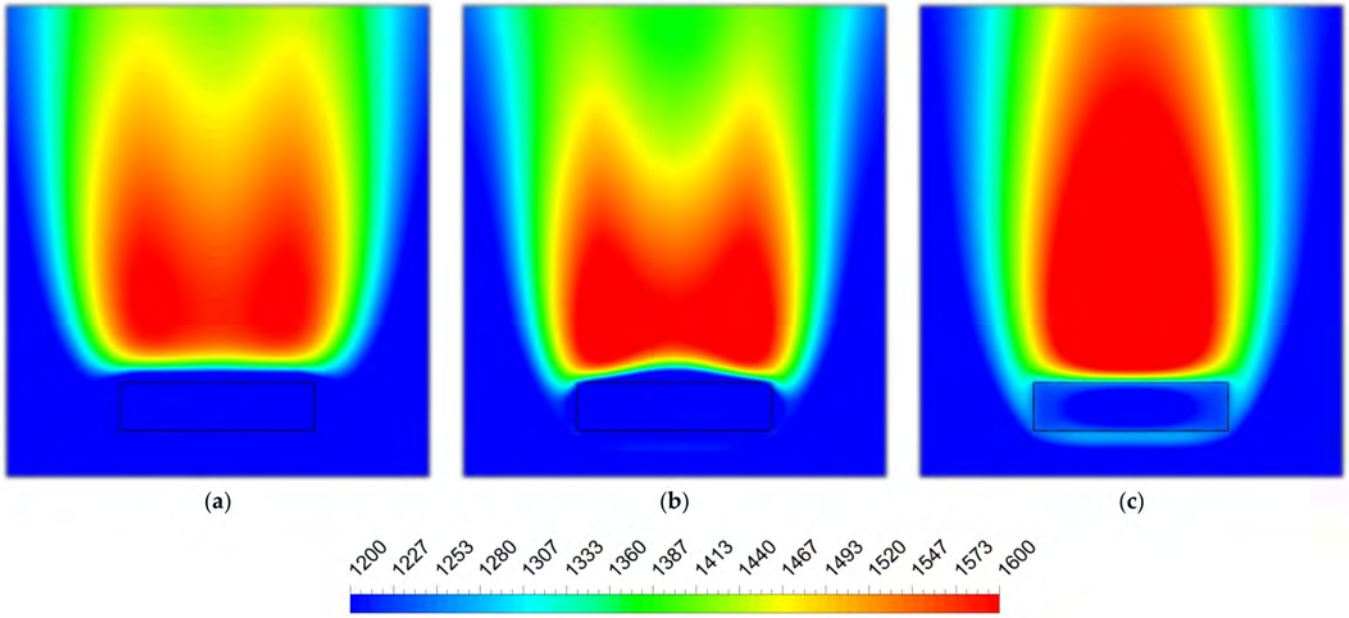

Figure 20. Temperature (in K) distribution at (**a**) t = 25 s, (**b**) 40 s and (**c**) 75 s.

4. Conclusions

The complexity of physical and chemical transformations taking place within biomass particles undergoing thermal decomposition is undeniably very high. Reproducing these processes with sufficient accuracy using numerical modeling and simulation requires a comparably detailed approach. Achieving the right balance between model sophistication and the associated computational effort is of great concern as well. Nevertheless, the modeling procedure presented herein is quite successful at reproducing the observable behavior of relatively large, heavily thermally loaded, biomass particles; this process is carried out with reasonable costs.

The implementation of the mathematical model for biomass decomposition presented in the first part of the study was performed taking advantage of the extensive capabilities of a commercial CFD software platform. The User-Defined Function was formulated such that the communication between the chemical-kinetic model and the CFD numerical model is bi-directional. Using dedicated subroutines, the program performed calculations for (1) the mass and energy sources for all mass transfer processes associated to the thermal decomposition of biomass and (2) the material properties and those of transport in solid volumes, extracting all necessary numerical data from the CFD solver. The calculation of heat and mass transfer, volatiles transport, and combustion, if conditions allow, enable char burn, etc., to all be performed within the solver. Of all the numerical tasks, the integration of chemical reaction mechanisms for gaseous species combustion seems to be the limiting factor in terms of computational performance.

The comparison of numerical results and experimental data used for validation is very good. The models qualitatively and quantitatively reproduce the experiments conducted by Lu [2] for a series of 9.5 mm cylindrical biomass samples (poplar), thermally decomposed in an oven specially designed and manufactured for this purpose. Both neutral and oxidizing conditions were successfully validated at low and high initial moisture levels too.

The global performance of the biomass thermal decomposition model developed in this research is remarkable, especially considering the fact that it relies on a relatively

simple chemical-kinetic scheme. The numerical model can be successfully used not only for accurate estimation of conversion process duration, either pyrolysis or combustion, or for estimating residual mass (i.e., char), but it can be applied as well for determining combustion temperatures in both key phases (volatiles burning, followed by char burning). Given the achieved level of accuracy, we can assume that the chemical composition of burnt gases might be properly predicted too, but this remains to be confirmed in future research.

The most important conclusion drawn from the analysis of all numerical data and their correspondence with experimental measurements is the following: in some cases it may be possible to apply one-dimensional or two-dimensional simplified models to obtain acceptable results in general engineering design; however, an accurate and thorough research of many apparently simple cases can be done only by using three-dimensional, unsteady numerical simulation methods that must be properly formulated physically and chemically to be as detailed and close to real phenomena as possible. Achieving high accuracy in numerical modeling cannot be done just by concentrating on aspects of physical and chemical transformations of biomass during thermal decomposition; the complete modeling of heat transport and, especially, mass transport, were found to be equally important.

Author Contributions: Conceptualization, I.V.I., F.P., and R.M.; methodology, I.V.I., F.P., R.M., and E.R.; software, R.M.; validation, R.M., F.P., and I.V.I.; formal analysis, E.R.; writing—original draft preparation, R.M.; writing—review and editing, I.V.I.; visualization, I.V.I.; funding acquisition, E.R. All authors have read and agreed to the published version of the manuscript.

Funding: This research was funded by the Romanian Executive Agency for Higher Education, Research, Development and Innovation Funding—UEFISCDI, grant number PN-III-P4-ID-PCE-2020-0008.

Institutional Review Board Statement: Not applicable.

Informed Consent Statement: Not applicable.

Acknowledgments: This work was carried out in the framework of the research project DREAM (Dynamics of the REsources and technological Advance in harvesting Marine renewable energy), supported by the Romanian Executive Agency for Higher Education, Research, Development and Innovation Funding—UEFISCDI, grant number PN-III-P4-ID-PCE-2020-0008.

Conflicts of Interest: The authors declare no conflict of interest.

References

1. Popescu, F.; Mahu, R.; Ion, I.V.; Rusu, E. A Mathematical Model of Biomass Combustion Physical and Chemical Processes. *Energies* **2020**, *13*, 6232. [CrossRef]
2. Lu, H. Experimental and Modeling Investigations of Biomass Particle Combustion. Ph.D. Thesis, Brigham Young University, Provo, UT, USA, 2006.
3. Gómez, M.A.; Porteiro, J.; Patiño, D.; Míguez, J.L. CFD modelling of thermal conversion and packed bed compaction in biomass combustion. *Fuel* **2014**, *117*, 16–732. [CrossRef]
4. Rezwanul, K.; Jamal, N. Numerical modelling of biomass combustion: Solid conversion processes in a fixed bed furnace. *AIP Conf. Proc.* **2017**, *1851*, 020029.
5. Porteiro, J.; Míguez, J.L.; Granada, E.; Moran, J.C. Mathematical modelling of the combustion of a single wood particle. *Fuel Process. Technol.* **2006**, *87*, 169–175. [CrossRef]
6. Karim, M.R.; Ovi, I.R.Q.; Naser, J. A CFD model for biomass combustion in a packed bed furnace, Proceedings of the 11th International Conference on Mechanical Engineering (ICME 2015). *AIP Publ.* **2016**, *1756*, 050026.
7. Hosseinzadeh, S.; Fattahi, A.; Sadeghi, S.; Rahmani, E.; Bidabadi, M.; Zarei, F.; Fei, X. Mathematical analysis of steady-state non-premixed multi-zonecombustion of porous biomass particles under counter-flow configuration. Renew. *Energy* **2020**, *159*, 705–725.
8. Lu, H.; Robert, W.; Peirce, G.; Ripa, B.; Baxter, L.L. Comprehensive Study of Biomass Particle Combustion. *Energy Fuels* **2008**, *22*, 2826–2839. [CrossRef]
9. Sousa, N.; Azevedo, J.L.T. Model simplifications on biomass particle combustion. *Fuel* **2016**, *184*, 948–956. [CrossRef]
10. Yang, Y.B.; Sharifi, V.N.; Swithenbank, J.; Ma, L.; Darvell, L.I.; Jones, M.J.; Pourkashanian, M.; Williams, A. Combustion of a Single Particle of Biomass. *Energy Fuels* **2008**, *22*, 306–316. [CrossRef]

11. Inamullah, M.; Xian, L.; Omar, D.D.; Jianjiang, W.; Bo, W.; Yiming, J.; Mei, Z.; Jingmei, L.; Fengyun, M.; Noor, R. Combustion kinetics and mechanism of biomass pellet. *Energy* **2020**, *205*, 117909.
12. Boriouchkine, A.; Jämsä-Jounela, S.L. Simplification of a Mechanistic Model of Biomass Combustion for On-Line Computations. *Energies* **2016**, *9*, 735. [CrossRef]
13. Roman, K.; Barwicki, J.; Hryniewicz, M.; Szadkowska, D.; Szadkowski, J. Production of Electricity and Heat from Biomass Wastes Using a Converted Aircraft Turbine AI-20. *Processes* **2021**, *9*, 364. [CrossRef]
14. Ansys Inc. *ANSYS 14.5 Documentation*; Analytical Graphics Inc: Canonsburg, PA, USA, 2018.
15. Green, D.W.; Perry, R.H. *Perry's Chemical Engineering Hanbook*, VIII ed.; McGraw-Hill: New York, NY, USA, 2008.
16. Senneca, O. Kinetics of pyrolysis, combustion and gasification of three biomass fuels. *Fuel Process. Technol.* **2007**, *88*, 87–97. [CrossRef]